Calorimetric and Magnetic Studies on a Ferromagnetic Phase Transition of the Metal-Assembled Complex MnCu(obbz)·H_2O#

Kaori Asano, Yuji Miyazaki, Wasuke Mori,† Keitaro Nakatani,††,## Olivier Kahn,†† and Michio Sorai*

Research Center for Molecular Thermodynamics, Graduate School of Science, Osaka University, Toyonaka, Osaka 560-0043

†Department of Chemistry, Faculty of Science, Kanagawa University, Tsuchiya 2946, Hiratsuka, Kanagawa 259-1205

††Laboratoire des Sciences Moléculaires, Institut de Chimie de la Matière Condenscée de Bordeaux, F-33608 Pessac, France

(Received December 13, 1999)

Heat capacities of the metal-assembled ferromagnet MnCu(obbz)·H_2O (obbz = oxamidobis(benzoato)) have been measured in the temperature region between 0.1 and 301 K by adiabatic calorimetry. A broad phase transition due to the three-dimensional ferromagnetic ordering was observed around 17 K. Above the transition temperature, a heat capacity tail arising from the short-range order characteristic of a low-dimensional magnet was found. The enthalpy and entropy gained by the phase transition are 227 J mol^{-1} and 12.7 J K^{-1} mol^{-1}, respectively. This entropy acquisition is very close to the value $R\ln 5$ (= 13.4 J K^{-1} mol^{-1}) expected for the spin manifold of the spin quantum number $S = 2$ ground state, where R stands for the gas constant. The thermal anomaly above the transition temperature can be accounted for in terms of the $S = 2$ two-dimensional ferromagnetic Heisenberg model rather than the one- or three-dimensional models. This suggests that this complex can be regarded as a two-dimensional ferrimagnet, in which strong antiferromagnetic interaction exists between a pair of Mn(II) ($S = 5/2$) and Cu(II) ($S = 1/2$) but the magnetic coupling between the pairs is very weak. Magnetic measurements for the complex revealed a bend of the hysteresis loop above the transition temperature and a magnetic relaxation below the transition temperature. These results lead to the conclusion that the broadness of the phase transition may be attributed to superparamagnetism caused by the fact that the present complex is prepared only in a fine powder.

Many molecule-based magnets have been recently prepared and extensively investigated.[1—31] One of the synthetic strategies is to assemble one-dimensional magnetic chains consisting of alternate arrangements of different metal ions. Even if, as is often the case, the intrachain interaction between the nearest neighbor metal ions is antiferromagnetic, the neighboring spins with different magnitudes do not cancel each other and consequently the chains may remain as being ferrimagnetic. The first successful molecule-based ferromagnet under such a concept was MnCu(pbaOH)$(H_2O)_3$ (pbaOH = 2-hydroxytrimethylenebis(oxamato)) systhesized by one of us.[1,2] This complex exhibits a ferromagnetic phase transition at T_c = 4.6 K.

Subsequently, under the same strategy, Kahn et al. synthesized the molecule-based ferromagnet MnCu(obbz)·H_2O (obbz = oxamidobis(benzoato)) with a higher T_c (= 14 K).[3,4] This complex is obtained by partial dehydration of MnCu(obbz)·$5H_2O$, which shows antiferromagnetism below T_N = 2.3 K.[4] Powder X-ray diffraction patterns and XANES and EXAFS spectra at Mn and Cu edges for MnCu(obbz)·$5H_2O$ and MnCu(obbz)·H_2O[4] have suggested that the structures of the two complexes resemble each other and that the Mn(II) and Cu(II) ions are located in octahedral and elongated tetragonal sites, respectively. Mn(II) and Cu(II) ions of both complexes are alternately bridged by oxamido and carboxylato groups of obbz to form one-dimensional chains. These chains are probably connected through bonds between Mn(II) and O belonging to adjacent chains, so that two- or three-dimensional packing occurs. One of five water molecules in MnCu(obbz)·$5H_2O$ is strongly coordinated and the other four water molecules are more weakly coordinated or non-coordinated. That is the reason for why MnCu(obbz)·$5H_2O$ easily changes to MnCu(obbz)·H_2O by dehydration.

Magnetic measurements[4] have revealed that the curve of $\chi_M T$ versus T for MnCu(obbz)·$5H_2O$ exhibits a sharp maximum due to three-dimensional antiferromagnetic ordering at T_N = 2.3 K, where χ_M is molar magnetic susceptibility per MnCu unit and T is temperature, while that for MnCu(obbz)·H_2O shows divergence towards T_c = 14 K due to three-dimensional ferromagnetic ordering. Furthermore, upon cooling, the $\chi_M T$–T curve for MnCu(obbz)·$5H_2O$ decreases and reaches a minimum around 40 K, which is

Contribution No. 18 from the Research Center for Molecular Thermodynamics.

Present address: Laboratoire de Photophysique et de Photochimie Supra- et Macromoleculaires, Ecole Normale Superieure de Cachan, 61 Avenue du President Wilson, F-94235 Cachan Cedex, France.

characteristic of ferrimagnetic chains with antiferromagnetic coupling. Also, the $\chi_M T$–T curve for MnCu(obbz)·H_2O decreases upon cooling and has a minimum around 120 K, which is expected for ferrimagnetic chains but is attributed to two- or three-dimensional rather than one-dimensional structures. Under applied magnetic field, both complexes give rise to the saturation magnetization corresponding to a resultant spin quantum number $S = 2$ per MnCu unit.

In the previous study,[32] we reported heat capacities of the metal-assembled antiferromagnet MnCu(obbz)·$5H_2O$ determined by adiabatic calorimetry, which is one of the powerful methods for investigation of magnetic properties of substances. We have revealed that this complex exhibits an antiferromagnetic phase transition at $T_N = 2.18$ K and a hump above T_N arising from the short-range order characteristic of low-dimensional magnets. This hump was well accounted for by the high-temperature series expansion for an $S = 2$ one dimensional Heisenberg ferromagnet. This suggests that MnCu(obbz)·$5H_2O$ behaves as a one-dimensional ferrimagnet, in which strong antiferromagnetic coupling exists between a pair of spins of Mn(II) ($S = 5/2$) and Cu(II) ($S = 1/2$) but the magnetic interaction is very weak between the pairs. The entropy acquisition due to the magnetic transition also supports this interpretation.

This time we measured heat capacities of the metal-assembled ferromagnet MnCu(obbz)·H_2O with adiabatic calorimeters. We observed a ferromagnetic phase transition expected from the magnetic measurements[3,4] and a thermal anomaly due to the short-range order characteristic of low-temperature magnets. We also found unusual features in this ferromagnetic phase transition by performing magnetization measurements. In this paper, we report precise and accurate thermodynamic quantities associated with the phase transition and discuss the mechanism of the phase transition from the calorimetric and magnetic experiments.

Experimental

Sample Preparation. The starting complex MnCu(obbz)·$5H_2O$ was synthesized by a method described elsewhere.[3,4] In accordance with its thermogravimetric analysis,[32] the pentahydrate complex was spread in a Petri dish and dehydrated in an electric furnace controlled at 70 °C for 2 h, 80 °C for 30 min, and 100 °C for 1 h. The complex thus treated was kept in a desiccator with silica gel for a few days to stabilize the dehydrated structure. The result of the elemental analysis for the sample thus obtained is as follows. Calcd for MnCu(obbz)·H_2O ($C_{16}H_{10}N_2O_7CuMn$): C, 41.71; H, 2.19; N, 6.08%. Found: C, 41.90; H, 2.05; N, 6.21%.

Heat Capacity Measurement. Two types of adiabatic calorimeters were employed for heat capacity measurements of MnCu(obbz)·H_2O depending on the temperature range. A very-low-temperature adiabatic calorimeter workable with a $^3He/^4He$ dilution refrigerator[33] was used for the measurement in the temperature range from 0.1 to 20 K. The sample with the mass of 5.00464 g was loaded into a gold-plated copper cell together with 4.75443 g of silicone oil (Toshiba Silicone, TSF433) to facilitate thermal equilibration. The measurement in the temperature region between 11 and 301 K was performed with a low-temperature adiabatic calorimeter for small samples.[34] In this case, only 0.60218 g of the sample was put into a 1.2 cm^3 gold-plated copper cell. Helium-4 gas under atmospheric pressure was filled into the cell to aid thermal equilibration. Buoyancy correction for the sample mass was made by assuming a density[4] of 1.9 g cm^{-3}.

Magnetic Measurement. Magnetic measurements for MnCu(obbz)·H_2O were carried out with a SQUID magnetometer (Quantum Design, MPMS-5S). Field cooled magnetizations of the sample at 20, 100, and 1000 G were measured between 4 and 30 K. Hysteresis loops of the sample were recorded at 1.9, 5, 8, 14, 20, and 30 K. AC magnetizations of the sample at 1, 10, and 100 Hz were measured from 4 to 30 K.

Powder X-Ray Diffraction. The powder X-ray diffraction pattern of MnCu(obbz)·H_2O was recorded at room temperature with a diffractometer (Rigaku Denki Co., Ltd., Model Rad-Roc). The range of reflection angle was $3° < 2\theta < 90°$ and the scanning speed was 3 ° min^{-1}.

Results and Discussion

Heat Capacity. The molar heat capacities of MnCu(obbz)·H_2O are listed in Table 1 and shown in Fig. 1. A very broad thermal anomaly was found around 17 K. The temperature of this anomaly is a little bit higher than the ferromagnetic phase transition temperature 14 K at which the magnetic susceptibilities $\chi_M T$ diverges,[4] but this anomaly can be regarded as a ferromagnetic phase transition. Moreover, above the transition temperature we observed a heat capacity tail arising from the short-range order characteristic of low-dimensional magnets. Although a structural phase transition was found at 268.4 K in MnCu(obbz)·$5H_2O$,[32] there was no

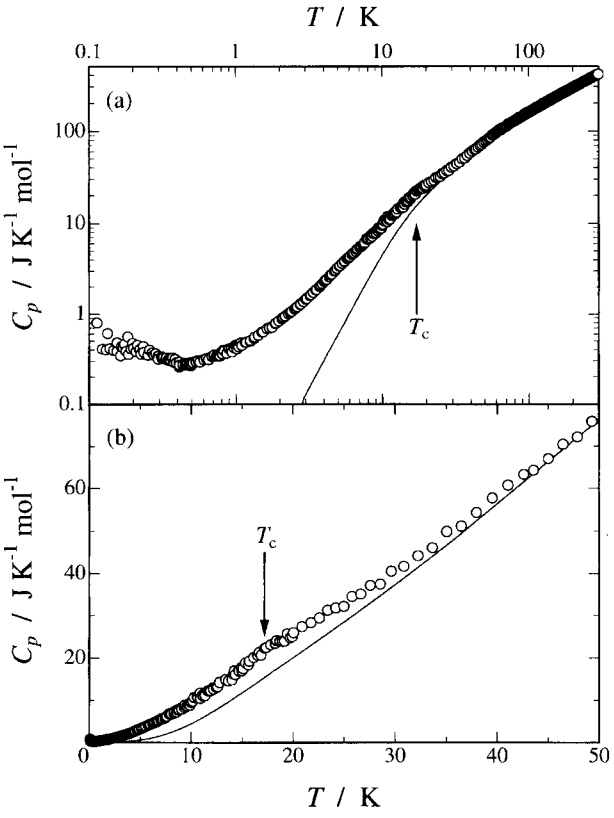

Fig. 1. Molar heat capacities of MnCu(obbz)·H_2O on (a) logarithmic and (b) normal scales. Solid curve indicates the normal heat capacities.

Table 1. Molar Heat Capacities of MnCu(obbz)·H_2O (M = 460.75 g mol^{-1})
Data in Series 1—6 and Series 7 and 8 were collected by use of different adiabatic calorimeters.

T/K	C_p/J K^{-1} mol^{-1}	T/K	C_p/J K^{-1} mol^{-1}	T/K	C_p/J K^{-1} mol^{-1}	T/K	C_p/J K^{-1} mol^{-1}
Series 1		0.321	0.326	3.917	2.159	2.363	1.043
0.113	0.803	0.346	0.306	4.049	2.281	2.575	1.168
0.134	0.611	0.413	0.258	4.198	2.412	2.790	1.297
0.155	0.482	0.453	0.271	4.371	2.576	3.020	1.460
0.166	0.435	0.497	0.267	4.553	2.747	3.267	1.628
0.175	0.464	0.502	0.276	4.740	2.980	3.535	1.841
0.184	0.561			4.937	3.200	3.822	2.074
0.198	0.474	Series 4		5.141	3.379	4.132	2.369
0.214	0.452	0.226	0.358	5.352	3.626	4.465	2.687
0.235	0.437	0.277	0.350	5.571	3.857	4.824	3.048
0.258	0.398	0.296	0.340	5.797	4.141	5.185	3.423
0.285	0.361	0.316	0.318	6.035	4.355	5.547	3.806
0.311	0.332	0.333	0.316	6.249	4.592	5.930	4.239
0.335	0.322	0.349	0.305	6.439	4.759	6.340	4.666
0.356	0.320	0.363	0.303	6.635	4.948	6.743	5.183
0.372	0.323	0.378	0.290	6.835	5.255	7.143	5.633
0.386	0.313	0.395	0.287	7.041	5.486	7.559	6.088
0.487	0.286	0.413	0.291	7.243	5.639	7.991	6.704
0.513	0.291	0.414	0.271	7.435	5.817	8.388	7.370
0.536	0.295	0.437	0.274	7.639	6.179	8.739	7.770
0.554	0.303	0.455	0.285	7.866	6.783	9.078	8.193
0.570	0.292	0.470	0.283	8.104	6.780	9.426	8.841
0.605	0.311	0.488	0.270	8.345	6.966	9.744	9.093
0.632	0.320	0.515	0.286	8.592	7.269	10.02	9.526
0.654	0.309	0.537	0.294	8.846	7.760	10.31	10.67
0.689	0.335	0.714	0.338	9.107	7.900	10.61	10.90
0.716	0.353	0.742	0.347	9.368	8.293	10.91	11.72
0.742	0.338	0.762	0.341	9.634	8.655	11.82	12.38
0.783	0.341	0.802	0.378	9.909	8.850	12.17	13.00
0.811	0.372	0.812	0.359	10.18	9.802	12.58	13.30
0.835	0.390	0.943	0.378	10.68	10.58	13.38	14.87
		1.017	0.438	10.92	10.46	14.23	16.93
Series 2				11.14	11.28	14.66	17.11
0.825	0.396	Series 5		11.39	11.17	15.12	17.45
0.868	0.366	0.994	0.452	11.66	12.25	15.62	18.32
0.896	0.411	1.020	0.409	11.93	12.27	16.14	20.09
0.924	0.401	1.048	0.433	12.20	12.64	16.68	21.31
0.974	0.421	1.101	0.449	12.50	13.06	17.24	22.32
1.010	0.451	1.178	0.486	12.79	14.23	17.82	23.11
1.083	0.477	1.260	0.509	13.67	14.61	18.42	24.14
		1.351	0.556	14.01	14.88	18.96	23.97
Series 3		1.513	0.631	14.35	16.05	19.44	25.72
0.123	0.408	1.641	0.691	14.68	16.94	19.93	25.03
0.131	0.400	1.773	0.715	15.00	16.97		
0.139	0.414	1.876	0.787	15.33	18.83	Series 7	
0.147	0.394	1.972	0.838	16.88	20.68	11.19	10.98
0.155	0.385	2.073	0.888	18.25	23.44	11.85	12.16
0.164	0.344	2.183	0.952	18.73	23.95	12.60	13.22
0.171	0.423	2.299	1.007	19.73	24.80	13.40	14.90
0.179	0.386	2.419	1.075			14.17	16.21
0.186	0.355	2.536	1.141	Series 6		14.92	17.65
0.193	0.409	2.641	1.204	1.160	0.487	15.71	19.23
0.200	0.418	2.764	1.280	1.255	0.498	16.53	20.64
0.209	0.379	2.912	1.376	1.342	0.537	17.39	22.47
0.221	0.400	3.067	1.489	1.424	0.581	18.27	23.47
0.236	0.375	3.228	1.604	1.542	0.637	19.18	23.97
0.252	0.348	3.396	1.738	1.703	0.708	20.05	25.98
0.270	0.371	3.572	1.859	1.884	0.793	20.89	27.41
0.296	0.315	3.757	2.009	2.125	0.919	21.76	28.31

Table 1. (Continued)

T / K	C_p / $JK^{-1}mol^{-1}$	T / K	C_p / $JK^{-1}mol^{-1}$	T / K	C_p / $JK^{-1}mol^{-1}$	T / K	C_p / $JK^{-1}mol^{-1}$
22.59	29.45	113.72	180.4	250.86	355.1	156.47	236.9
23.41	31.23	115.82	181.7	253.40	358.3	158.53	239.4
24.21	31.77	117.93	185.7	255.95	360.3	160.60	242.3
24.99	32.15	120.05	188.1	258.52	362.7	162.67	246.0
25.79	34.50	122.19	191.2	261.09	367.4	164.76	248.8
26.64	35.08	124.34	195.3	263.68	369.5	166.85	249.4
27.57	37.14	126.51	196.3	266.27	372.8	168.95	253.4
28.57	37.44	128.69	198.8	268.88	374.5	171.05	256.9
29.63	40.51	130.88	202.0	271.50	376.0	173.17	257.8
30.88	41.68	133.08	206.4	274.13	380.8	175.29	262.0
32.25	44.22	135.31	209.6	276.78	384.1	177.43	263.9
33.65	46.06	137.54	210.8	279.44	387.2	179.57	267.7
35.06	49.88	139.79	214.7	282.10	389.4	181.72	270.5
36.47	51.12	142.06	219.4	284.78	391.7	183.88	273.0
37.96	54.27	144.34	222.0	287.47	396.2	186.15	273.7
39.52	57.70	146.49	223.4	290.16	399.8	188.24	277.1
41.07	60.75	148.51	226.1	292.86	402.1	190.43	280.4
42.61	63.28	150.55	229.4	295.58	405.5	192.63	282.4
43.57	64.26	152.59	231.6	298.30	408.3	194.83	286.8
45.03	67.04	154.64	233.1	301.03	414.4	197.05	289.3
46.47	70.42	156.71	238.0			199.28	290.8
47.89	72.20	158.78	240.7	Series 8		201.51	294.9
49.30	75.92	160.86	243.2	79.60	128.3	203.76	298.4
50.74	78.43	162.95	244.7	81.62	130.9	206.01	299.2
52.22	81.01	165.06	248.3	83.62	134.9	208.28	300.2
53.68	83.97	167.17	251.5	85.61	137.8	210.56	306.1
55.13	86.54	169.30	254.2	87.58	141.3	212.84	308.2
56.57	91.33	171.43	256.8	89.55	143.5	215.13	310.0
58.01	92.84	173.57	260.5	91.50	146.9	217.43	314.8
59.44	95.22	175.73	260.7	93.45	150.5	219.75	316.2
60.86	98.76	177.90	265.8	95.39	153.1	222.07	318.7
62.28	101.2	180.07	265.6	97.33	155.0	224.40	320.6
63.53	104.3	182.27	267.8	99.26	159.2	229.09	328.6
64.53	103.6	184.47	269.3	101.20	161.2	231.44	331.0
65.56	106.9	186.68	274.7	103.13	164.1	233.81	334.8
66.85	108.6	188.90	277.9	105.05	167.2	236.19	338.1
68.40	110.2	191.13	279.7	106.98	170.2	238.57	339.0
69.97	111.9	193.37	285.5	108.91	172.9	240.97	341.8
71.54	115.9	195.62	287.6	110.84	175.3	243.38	344.6
73.13	120.4	197.88	290.5	112.77	179.4	245.79	347.4
74.73	121.4	200.15	291.5	114.71	180.6	248.22	352.0
76.34	123.6	202.44	294.9	116.64	184.0	250.65	352.7
77.97	126.3	204.73	297.5	118.58	186.2	253.09	356.4
79.60	128.3	207.04	299.7	120.53	188.5	255.54	359.5
81.24	131.7	209.35	302.8	122.48	191.0	258.01	363.2
82.89	133.3	211.69	308.5	124.43	194.1	260.49	367.8
84.56	137.5	214.06	309.9	126.39	198.9	262.99	370.4
86.23	140.2	216.43	310.8	128.35	199.5	265.50	373.1
87.92	141.6	218.82	314.1	130.32	202.3	268.01	376.0
89.62	143.6	221.22	316.5	132.29	203.3	270.54	378.2
91.44	147.0	223.63	319.3	134.27	207.7	273.08	382.0
93.41	151.3	226.05	321.3	136.25	209.9	275.63	382.3
95.40	154.0	228.48	327.1	138.24	214.3	278.19	385.8
97.39	156.9	230.92	330.5	140.24	214.8	280.75	389.9
99.39	158.3	233.38	332.9	142.24	218.2	283.33	392.8
101.40	161.4	235.84	337.5	144.25	220.2	285.91	395.8
103.42	166.1	238.31	338.8	146.27	222.6	288.51	398.2
105.46	166.5	240.80	342.9	148.30	226.6	291.11	402.8
107.51	170.9	243.30	346.4	150.33	229.1	293.72	403.2
109.57	173.3	245.81	348.7	152.37	232.8	296.34	406.8
111.64	177.5	248.33	351.3	154.41	233.1	298.97	410.2

such a thermal anomaly in the case of MnCu(obbz)·H_2O.

The heat capacities below 0.5 K imply an additional thermal anomaly. It is very likely that the monohydrate prepared by partial dehydration of the pentahydrate may involve fairly large amounts of defects and imperfections in the crystal lattice. Consequently, we assume that this heat capacity anomaly would originate in the physical and/or chemical impurities though they are closely related to MnCu(obbz)·H_2O.

Magnetization. The field cooled magnetizations of MnCu(obbz)·H_2O recorded at the magnetic field of 20, 100, and 1000 G are plotted in Fig. 2 as a function of temperature. One can see in Fig. 2 that the spontaneous magnetization occurred below T_c = 14, 18, and 22 K when the applied magnetic field was 20, 100, and 1000 G, respectively. This fact reveals that the present complex exhibits a ferromagnetic phase transition as reported previously.[3,4] The transition temperature in the magnetization measurement with 20 G is in good agreement with that with 0.1 G.[3,4] It is very interesting that the transition temperature remarkably depends on the applied magnetic field, even though the field is not so large. On the other hand, the magnetization curves do not sharply fall at T_c when the temperature is increased. This point will be discussed later.

Figure 3 indicates the hysteresis loops of the monohydrate at 1.9, 5, 8, 14, 20, and 30 K. Hysteresis was observed below 14 K, at which the magnetic phase transition occurred. This hysteresis became larger as the temperature was lowered. The curve of the magnetization M versus applied magnetic field H becomes linear at 30 K as seen in paramagnetic materials. However, the M–H curve at 20 K is nonlinear although the temperature is higher than T_c. This feature is different from the case of normal paramagnetic substances.

Figure 4 shows the real and imaginary parts of the a.c. magnetization of the sample measured with 1, 10, and 100 Hz. Magnetic relaxation was found around 9 K, which is lower than T_c. The peak temperature of the imaginary part did not exhibit explicit frequency dependence.

Determination of Normal and Excess Heat Capacities. In order to elucidate the nature of the present ferromagnetic

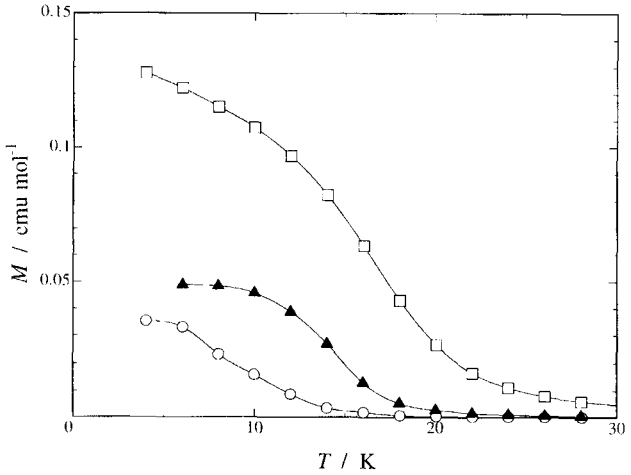

Fig. 2. Field cooled magnetizations of MnCu(obbz)·H_2O. ○: 20 G, ▲: 100 G, □: 1000 G.

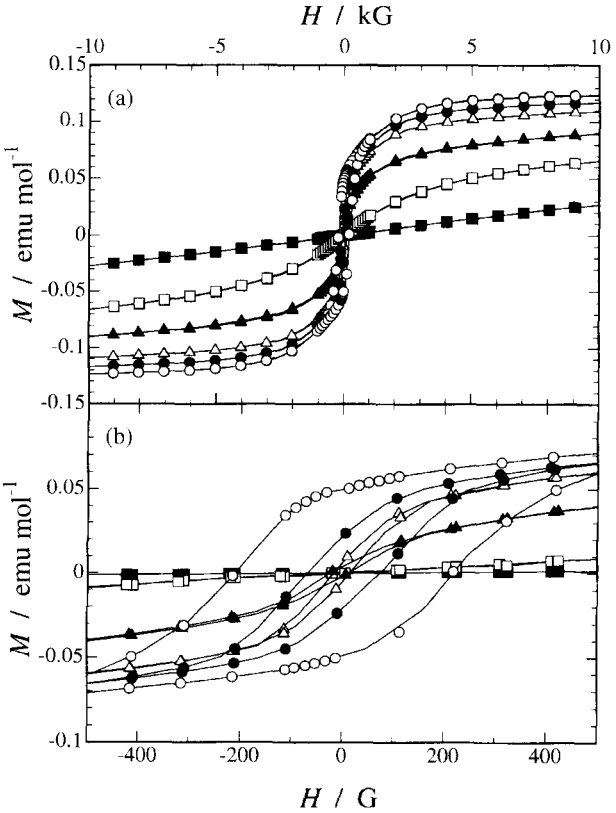

Fig. 3. Hysteresis loops of MnCu(obbz)·H_2O (a) over the whole magnetic field range studies here and (b) in the vicinity of zero magnetic field. ○: 1.9 K, ●: 5 K, △: 8 K, ▲: 14 K, □: 20 K, ■: 30 K.

phase transition in detail, we estimated the excess heat capacities of MnCu(obbz)·H_2O by subtracting the normal heat capacities from the total heat capacities. In the present case, an effective frequency distribution method[35] was used for determination of the normal heat capacities. This complex contains 37 atoms per formula unit, and hence the number of degrees of freedom is 111. Of these, three degrees of freedom are assigned to translation, three to overall rotation, and the remaining 105 to intramolecular vibration. We used the known 79 frequencies of intramolecular vibration in reference to the values assigned for MnCu(obbz)·$5H_2O$.[32] The contribution of these modes to the normal heat capacity is expressed in terms of the Einstein model. The remaining unknown 26 modes of intramolecular vibration, six modes of lattice vibration (translation and libration), and the $(C_p - C_V)$ correction are approximated by a continuous frequency spectrum spanning the range 0—700 cm^{-1}, which consists of two Debye distributions and three continuous and constant distributions. Reasonable frequency distributions are determined by nonlinear least squares fitting to the heat capacity data in the 23—149 K temperature range. The observed heat capacities above the magnetic transition temperature include the contribution from the short-range order. This contribution was approximated by a term proportional to T^{-2} for the fitting.

The normal heat capacity curve thus derived is drawn in

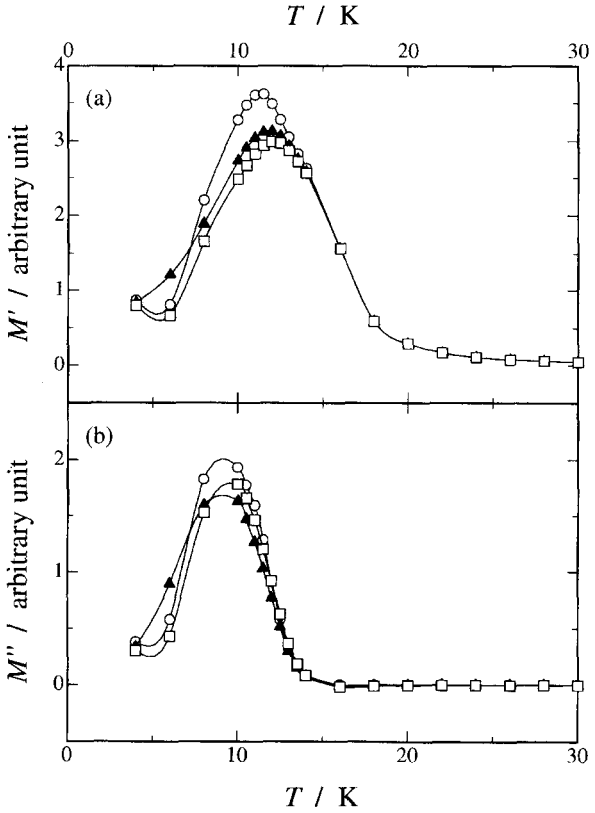

Fig. 4. Real (a) and imaginary (b) parts of a.c. magnetizations of MnCu(obbz)·H_2O. ○: 1 Hz, ▲: 10 Hz, □: 100 Hz.

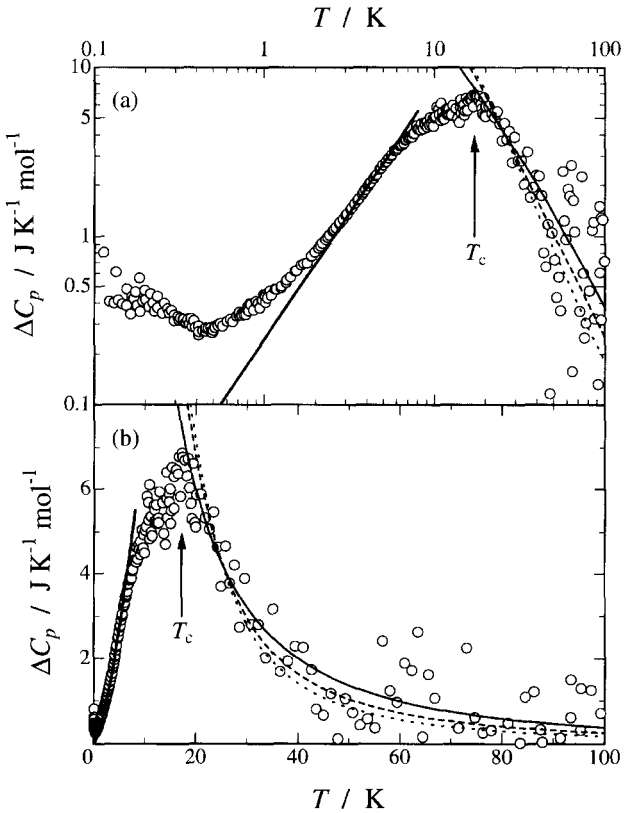

Fig. 5. Excess heat capacities of MnCu(obbz)·H_2O on (a) logarithmic and (b) normal scales. Solid, dashed, and dotted curves indicate the theoretical heat capacity curves estimated by the high-temperature series expansion for $S = 2$ two-dimensional ferromagnetic Heisenberg models of honeycomb, square, and triangular lattices with $J/k_B = 2.6$, 1.8, and 1.1 K, respectively. Thick solid curve drawn below 8 K shows the heat capacities derived from the spin wave theory for three-dimensional ferromagnets.

Fig. 1 by a solid curve. The proportional coefficient of the T^{-2} term was estimated to be 2.79 kJ K mol^{-1}. The excess heat capacities were calculated by subtracting the normal heat capacities from the observed ones. The obtained excess heat capacities are plotted against temperature in Fig. 5. A broad but obvious heat capacity peak centered around 17 K can be seen. The thermal anomaly due to the short-range order of the spin arrangement is recognized more clearly above the transition temperature. However, this anomaly is not so prominent in comparison with that of MnCu(obbz)·$5H_2O$.[32]

Transition Enthalpy and Entropy. One can evaluate the enthalpy and entropy gains due to the magnetic phase transition from the excess heat capacities. As mentioned above, an additional thermal anomaly was found below 0.5 K. If this thermal anomaly is ignored, the evaluation of the transition enthalpy and entropy can be performed as follows. The enthalpy and entropy gained from 0 to 3 K were calculated on the basis of the spin wave theory described later. Those between 3 and 67 K were evaluated by directly integrating the excess heat capacities with respect to T and $\ln T$, respectively. The enthalpy and entropy acquired above 67 K were estimated on the basis of the T^{-2} term. The resulting enthalpy and entropy acquisitions were determined to be 226 J mol^{-1} and 11.9 J K^{-1} mol^{-1}, respectively.

If the thermal anomaly below 0.5 K is included as the magnetic effect, the enthalpy and entropy gains were evaluated by the sum of the direct integration of the excess heat capacities from 0.1 to 67 K with respect to T and $\ln T$ and the contribution above 67 K calculated by the T^{-2} term. Here, the contribution below 0.1 K was not estimated because of the absence of information about the temperature dependence of the excess heat capacities. In this case, the transition enthalpy and entropy amounted to 227 J mol^{-1} and 12.7 J K^{-1} mol^{-1}, respectively.

Since it is very likely that the thermal anomaly below 0.5 K arises from the defects and imperfections in the crystal lattice, the contribution of this thermal anomaly should be included in the estimation of the magnetic enthalpy and entropy gains. Therefore, we can regard the latter case as providing closer values to the true magnetic enthalpy and entropy.

Mechanism of the Ferromagnetic Phase Transition. While MnCu(obbz)·$5H_2O$ has most likely a one-dimensional network structure, MnCu(obbz)·H_2O should have a two- or three-dimensional network structure composed of ferrimagnetic chains in which Mn(II) and Cu(II) ions are alternately bridged by two different groups: oxamido and carboxylato.[4]

The entropy acquisition 12.7 J K^{-1} mol^{-1} due to the ferromagnetic phase transition is close to $R\ln 5$ (= 13.4 J K^{-1} mol^{-1}) expected for a $S = 2$ spin system (R: the gas

constant). This means that the ferrimagnetic chains in MnCu(obbz)·H_2O can be regarded, at low temperatures, as $S = 2$ pseudo-ferromagnetic chains made up of two different antiferromagnetically coupled spins, $S = 5/2$ for Mn(II) and $S = 1/2$ for Cu(II). The slight difference between the experimental and theoretical values would probably be due to the absence of evaluation of the entropy gain below 0.1 K. Since the whole entropy gain for the Mn(II)–Cu(II) system amounts to $R\ln(6\times2)$ (= 20.7 J K^{-1} mol^{-1}), the remaining entropy of $R\ln(12/5)$ (= 7.3 J K^{-1} mol^{-1}) would be probably acquired at higher temperatures by thermal excitation from the ground $S = 2$ level to the excited $S = 3$ spin level as in the case of MnCu(obbz)·$5H_2O$.[32]

We attempted to compare the thermal anomaly still existing above the transition temperature with several $S = 2$ ferromagnetic Heisenberg models.[36–39] In the case of MnCu(obbz)·$5H_2O$, the heat capacity anomaly above the magnetic transition temperature could be expressed by the $S = 2$ one-dimensional ferromagnetic Heisenberg model with the exchange interaction $J/k_B = 0.75$ K,[32] where k_B denotes the Boltzmann constant. As to MnCu(obbz)·H_2O, however, agreement between the experimental and theoretical values was poor when a $S = 2$ one-dimensional ferromagnetic Heisenberg model[36] was applied. Similarly, poor agreement was obtained for $S = 2$ three-dimensional ferromagnetic Heisenberg models.[37,38] We could more successfully fit $S = 2$ two-dimensional ferromagnetic Heisenberg models[37–39] to the thermal anomaly. This feature is demonstrated in Fig. 5. The best fit was obtained for the $S = 2$ two-dimensional Heisenberg model of honeycomb lattice with $J/k_B = 2.6$ K. We could also fit the thermal anomaly to the $S = 2$ two-dimensional Heisenberg models of square and triangular lattices with $J/k_B = 1.8$ K and $J/k_B = 1.1$ K, respectively. These two models also reproduce well the observed thermal anomaly. The exchange interaction parameters thus determined are larger than that of MnCu(obbz)·$5H_2O$.[32] This implies that the crystal packing in MnCu(obbz)·H_2O is more compact owing to the lack of four water molecules. Therefore, it turns out from the present study that MnCu(obbz)·H_2O takes a two-dimensional magnetic structure above the transition temperature.

We applied spin wave theory to the magnetic heat capacities ΔC_p below the transition temperature. Spin wave theory is a good approximation describing the low-temperature magnetic properties of materials, in the same sense as the lattice heat capacity at low temperatures is well approximated by the Debye theory. The low-temperature heat capacity due to the spin wave excitation, C_{SW}, is represented by the following equation,[40]

$$C_{SW} \propto T^{d/n}, \tag{1}$$

where d denotes the dimensionality and n is defined as the exponent in the dispersion relation: $n = 1$ for antiferromagnets and $n = 2$ for ferromagnets. We tried to fit the following expression to the magnetic heat capacities in the temperature range from 3 to 5 K to investigate the temperature dependence of the magnetic heat capacities at low temperatures:

$$\Delta C_p = AT^{\alpha}. \tag{2}$$

The best fit was obtained for $\alpha = 1.38 \approx 3/2$ and $A = 0.243$ J $K^{-5/2}$ mol^{-1}. The spin wave heat capacity thus derived is drawn in Fig. 5 by thick solid curves below 8 K. This result suggests that the spin system would order three-dimensionally and ferromagnetically below the magnetic transition temperature. This situation is quite normal, because two-dimensional Heisenberg spin systems give rise to a phase transition only when weak three-dimensional magnetic interaction exists.

As can be seen in Fig. 5(a), the magnetic heat capacities of the complex deviate upwards from the spin wave heat capacity line below 3 K. As described above, this anomaly would be plausibly ascribed to the presence of a small amount of physical and/or chemical impurities such as imperfect ferrimagnetic chains which occurred during the sample preparation. This is also the case for MnCu(obbz)·$5H_2O$.[32] However, the heat capacity anomaly for MnCu(obbz)·H_2O is much larger than that for MnCu(obbz)·$5H_2O$. The partial dehydration from the pentahydrate compound to the monohydrate one seems to bring about a noticeable amount of defects and imperfections in the crystal lattice of MnCu(obbz)·H_2O.

In what follows, we pay attention to the nature of the ferromagnetic phase transition in MnCu(obbz)·H_2O. As revealed by the heat capacity and magnetization measurements, the observed ferromagnetic phase transition is very broad in contrast to the sharp antiferromagnetic phase transition found in MnCu(obbz)·$5H_2O$.[32] We shall consider several possibilities responsible for the broadening of this phase transition.

(i) *Amorphization.* MnCu(obbz)·H_2O was prepared by partial dehydration of MnCu(obbz)·$5H_2O$. This dehydration process is still difficult even under mild conditions, so that it would be possible that an amorphous state is formed. In such a case, the phase transition peak is expected to turn to a broad one. This possibility was checked by powder X-ray diffraction. The diffraction pattern of MnCu(obbz)·H_2O at 300 K is shown in Fig. 6 together with that of MnCu(obbz)·$5H_2O$.[32] Both diffraction patterns closely resemble each other as expected from the previous powder X-ray diffraction study.[4] This means that the two crystal structures are essentially identical. All the Bragg reflection peaks of MnCu(obbz)·H_2O shift slightly to lower angles in comparison to those of MnCu(obbz)·$5H_2O$. This weak shrinkage effect in MnCu(obbz)·H_2O is caused by elimination of four water molecules from MnCu(obbz)·$5H_2O$. Although the Bragg reflection peaks were slightly broad in both MnCu(obbz)·H_2O and MnCu(obbz)·$5H_2O$, no halos characteristic of amorphous materials were found. This slight broadening would be attributed to fine powder. Anyhow, the appearance of the Bragg reflection peaks in this sample clarifies that the present specimen is composed not of amorphous solid but of crystalline powder.

(ii) *Grain Size Effect.* For compounds made up of fine powder the phase transitions become broad, because their

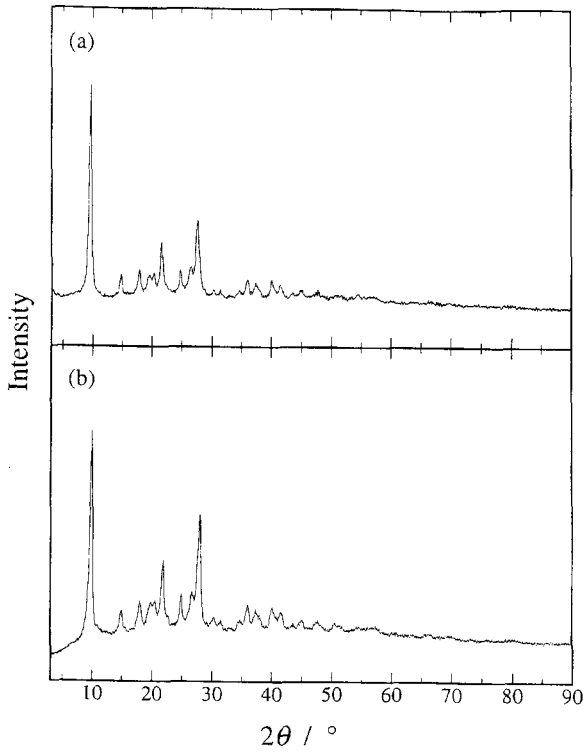

Fig. 6. Powder X-ray diffraction patterns of (a) MnCu(obbz)·H_2O and (b) MnCu(obbz)·$5H_2O$[32] at 300 K.

surface energy becomes larger as their surface area increases. Moreover, fine powder may give rise to a distribution of their transition temperatures owing to the distribution of the grain size. The monohydrate complex used in the present study as well as the original pentahydrate complex seemingly consists of fine powder. However, MnCu(obbz)·$5H_2O$ brought about a rather sharp phase transition in spite of fine powder.[32] When one carefully looks at Fig. 6, one notices that several reflection peaks of MnCu(obbz)·H_2O are relatively weak in comparison to those of MnCu(obbz)·$5H_2O$. This implies that the grain size of the MnCu(obbz)·H_2O crystal became smaller than that of the MnCu(obbz)·$5H_2O$ crystal through the partial dehydration. Therefore, this possibility is conceivable, though it may not be the main cause for the broadness of the phase transition peak.

(iii) *Superparamagnetism.* Fine particles are known to manifest different physical properties compared with the bulk. When ferromagnetic particles become smaller, a multidomain structure in a bulk is transformed into a single domain in a fine particle. When the magnetic anisotropy energy is not so large, the ferromagnetic fine powder behaves as if it were paramagnetic, the so-called "superparamagnetism". This superparamagnetism is closely related with the grain size effect in nature. As seen in Fig. 3, the magnitude of the hysteresis loops below T_c is extremely small in comparison to that of normal ferromagnetic compounds. Moreover, the magnetization recorded at 20 K, 3 K higher than T_c, still exhibits a bent form. Magnetic relaxation was also observed in this sample as seen in Fig. 4. These experimental results may reveal the features of superparamagnetism. In Fig. 4, no remarkable frequency dependence of the imaginary part of the a.c. magnetizations is seen. This might be due to a wide distribution of the magnetic relaxation times. Therefore, this possibility is the most plausible as a main cause of the broadness of the phase transition peak.

This work was partially supported by a Grant-in-Aid for Scientific Research on Priority Areas "Metal-Assembled Complexes" (Area No. 401/11136226) from the Ministry of Education, Science, Sports and Culture.

References

1 Y. Pei, M. Verdaguer, and O. Kahn, *J. Am. Chem. Soc.*, **108**, 7428 (1986).

2 O. Kahn, Y. Pei, M. Verdaguer, J. P. Renard, and J. Sletten, *J. Am. Chem. Soc.*, **110**, 782 (1988).

3 F. Lloret, K. Nakatani, Y. Journaux, O. Kahn, Y. Pei, and J. P. Renard, *J. Chem. Soc., Chem. Commun.*, **1988**, 642.

4 K. Nakatani, J. Y. Carriat, Y. Journaux, O. Kahn, F. Lloret, J. P. Renard, Y. Pei, J. Sletten, and M. Verdaguer, *J. Am. Chem. Soc.*, **111**, 5739 (1989).

5 J. S. Miller, J. C. Calabrese, A. J. Epstein, R. W. Bigelow, J. H. Zhang, and W. M. Reiff, *J. Chem. Soc., Chem. Commun.*, **1986**, 1026.

6 J. S. Miller, J. C. Calabrese, H. Rommelmann, S. R. Chittipeddi, J. H. Zhang, W. M. Reiff, and A. J. Epstein, *J. Am. Chem. Soc.*, **109**, 769 (1987).

7 J. S. Miller, A. J. Epstein, and W. M. Reiff, *Chem. Rev.*, **88**, 201 (1988).

8 J. S. Miller, A. J. Epstein, and W. M. Reiff, *Science*, **240**, 40 (1988).

9 J. S. Miller, A. J. Epstein, J. C. Calabrese, R. L. Harlow, D. A. Dixon, J. H. Zhang, W. M. Reiff, S. R. Chittipeddi, M. A. Selover, and A. J. Epstein, *J. Am. Chem. Soc.*, **112**, 5496 (1990).

10 A. Caneschi, D. Gatteschi, and R. Sessoli, *Acc. Chem. Res.*, **22**, 392 (1989).

11 A. Caneschi, D. Gatteschi, J. P. Renard, P. Rey, and R. Sessoli, *Inorg. Chem.*, **28**, 1976 (1989).

12 A. Caneschi, D. Gatteschi, J. P. Renard, P. Rey, and R. Sessoli, *Inorg. Chem.*, **28**, 3314 (1989).

13 Z. J. Zhong, N. Matsumoto, H. Ōkawa, and S. Kida, *Chem. Lett.*, **1990**, 87.

14 H. Tamaki, M. Mitsumi, K. Nakamura, N. Matsumoto, S. Kida, H. Ōkawa, and S. Iijima, *Chem. Lett.*, **1992**, 1975.

15 H. Tamaki, Z. J. Zhong, N. Matsumoto, S. Kida, M. Koikawa, N. Achiwa, Y. Hashimoto, and H. Ōkawa, *J. Am. Chem. Soc.*, **114**, 6974 (1992).

16 H. Miyasaka, N. Matsumoto, H. Ōkawa, N. Re, E. Gallo, and C. Floriani, *Angew. Chem., Int. Ed. Engl.*, **34**, 1446 (1995).

17 H. Miyasaka, N. Matsumoto, H. Ōkawa, N. Re, E. Gallo, and C. Floriani, *J. Am. Chem. Soc.*, **118**, 981 (1996).

18 N. Re, E. Gallo, C. Floriani, H. Miyasaka, and N. Matsumoto, *Inorg. Chem.*, **35**, 6004 (1996).

19 H. Miyasaka, N. Matsumoto, N. Re, E. Gallo, and C. Floriani, *Inorg. Chem.*, **36**, 670 (1997).

20 M. Kinoshita, P. Turek, M. Tamura, K. Nozawa, D. Shiomi, Y. Nakazawa, M. Ishikawa, M. Takahashi, K. Awaga, T. Inabe, and Y. Maruyama, *Chem. Lett.*, **1991**, 1225.

21 M. Takahashi, P. Turek, Y. Nakazawa, M. Tamura, K. Nozawa, D. Shiomi, M. Ishikawa, and M. Kinoshita, *Phys. Rev.*

Lett., **67**, 746 (1991).
22 M. Tamura, Y. Nakazawa, D. Shiomi, K. Nozawa, Y. Hosokoshi, M. Ishikawa, M. Takahashi, and M. Kinoshita, *Chem. Phys. Lett.*, **186**, 401 (1991).
23 Y. Nakazawa, M. Tamura, N. Shirakawa, D. Shiomi, M. Takahashi, M. Kinoshita, and M. Ishikawa, *Phys. Rev. B*, **46**, 8906 (1992).
24 M. Takahashi, M. Kinoshita, and M. Ishikawa, *J. Phys. Soc. Jpn.*, **61**, 3745 (1992).
25 R. Chiarelli, A. Rassat, and P. Pey, *J. Chem. Soc., Chem. Commun.*, **1992**, 1081.
26 R. Chiarelli, M. A. Novak, A. Rassat, and J. L. Tholence, *Nature*, **363**, 147 (1993).
27 T. Nogami, K. Tomioka, T. Ishida, H. Yoshikawa, M. Yasui, F. Iwasaki, H. Iwamura, N. Takeda, and M. Ishikawa, *Chem. Lett.*, **1994**, 29.
28 T. Ishida, H. Tsuboi, T. Nogami, H. Yoshikawa, M. Yasui, F. Iwasaki, H. Iwamura, N. Takeda, and M. Ishikawa, *Chem. Lett.*, **1994**, 919.
29 T. Nogami, T. Ishida, H. Tsuboi, H. Yoshikawa, H. Yamamoto, M. Yasui, F. Iwasaki, H. Iwamura, N. Takeda, and M. Ishikawa, *Chem. Lett.*, **1995**, 635.
30 K.Inoue and H. Iwamura, *J. Am. Chem. Soc.*, **116**, 3173 (1994).
31 T. Sugawara, M. M. Matsushita, A. Izuoka, N. Wada, N. Takeda, and M. Ishikawa, *J. Chem. Soc., Chem. Commun.*, **1994**, 1723.
32 K. Asano, K. Inoue, M. Nakano, Y. Miyazaki, M. Sorai, K. Nakatani, and O. Kahn, *Bull. Chem. Soc. Jpn.*, **72**, 1749 (1999).
33 S. Murakawa, T. Wakamatsu, M. Nakano, M. Sorai, and H. Suga, *J. Chem. Thermodyn.*, **19**, 1275 (1987).
34 Y. Kume, Y. Miyazaki, T. Matsuo, and H. Suga, *J. Phys. Chem. Solids*, **53**, 1297 (1992).
35 M. Sorai and S. Seki, *J. Phys. Soc. Jpn.*, **32**, 382 (1972).
36 T. de Neef, A. J. M. Kuipers, and K. Kopinga, *J. Phys. A*, **7**, L171 (1974).
37 G. S. Rushbrooke and P. J. Wood, *Mol. Phys.*, **1**, 257 (1958).
38 R. L. Stephenson, K. Pirnie, P. J. Wood, and J. Eve, *Phys. Lett.*, **27A**, 2 (1968).
39 K. Yamaji and J. Kondo, *J. Phys. Soc. Jpn.*, **35**, 25 (1973).
40 L. J. de Jongh and A. R. Miedema, *Adv. Phys.*, **23**, 1 (1974).